Numerical and experimental studies of pressure-controlled cavity expansion in completely decomposed granite soils of Hong Kong

S.Y. Wang [a,*], D.H. Chan [b,1], K.C. Lam [c,2], S.K.A. AU [d,3]

[a] Centre for Geotechnical and Materials Modelling, Department of Civil, Surveying and Environmental Engineering, The University of Newcastle, Callaghan, NSW 2308, Australia
[b] Department of Civil and Environmental Engineering, University of Alberta, Canada T6G 2W2
[c] Department of Building and Construction, City University of Hong Kong, Tat Chee Avenue, Kowloon, Hong Kong
[d] Department of Civil Engineering, The University of Hong Kong, Pokfulam Road, Hong Kong

ARTICLE INFO

ABSTRACT

Compaction grouting is the injection of a viscous grout into a soil under high pressure, which then densifies the surrounding soil by reducing void space. Laboratory and field tests of compaction grouting have been carried out. In this paper, a numerical model is used to simulate the compaction grouting process with the primary purpose of investigating relationships among various control parameters, such as injection pressure, void ratio and excess pore water pressure at various radial distances from the injection point. The compaction process is treated as a cavity expansion process in the numerical simulation. The soil is modelled with an elasto-plastic Mohr–Coulomb model using the commercial finite element program ABAQUS. In addition to numerical simulations, pressure-controlled cavity expansion laboratory tests were carried out on completely decomposed granite (CDG) soil specimens. Data collected from laboratory tests are compared with the finite element simulation to validate the finite element analyses. Factors that control the compaction process, such as the coefficient of earth pressure (K), initial void ratio, number of loading cycles and effective confining pressure, are explored in the numerical simulations.

Crown Copyright © 2010 Published by Elsevier Ltd. All rights reserved.

1. Introduction

In general, compaction grouting involves injecting an expanding bulb of highly viscous grout with high internal friction into a compressible soil. This process physically displaces the soil particles and moves them closer together, thus achieving controlled densification. The basic principle and procedure of compaction grouting have been described by Graf [1]. The applicability of the procedure in the field has been evaluated and experimental studies related to the procedure have been reported by Warner and Brown [2]. Ideally, compaction grouting can be simplified as a cavity expansion process [3]. The expansion of a cavity in an infinite medium is a well known problem in applied mechanics and is of particular interest to geotechnical engineers [4–6]. Several solutions to the problem have been proposed for a number of idealised materials [7,8]. The three dimensional problem is usually simplified into two or one dimension by considering axisymmetric and plane strain conditions. During compaction, excess pore water pressure will develop because the soil is saturated and the void space is reduced under the compaction pressure. This excess pore water pressure will be subsequently dissipated by draining water radially away from the expanding cavity. The consolidation process that follows the compaction is responsible for most of the decrease in the void ratio in the surrounding soil, which leads to an increase in the strength of the material [9].

Cavity expansion has been used to study many geotechnical problems. For example, the state of stress and strain induced in the soil by cone penetrometers, driven piles, and other instruments has commonly been estimated by approximate analytical techniques, such as cavity expansion [10–15]. Most analytical solutions describing the cavity expansion process are derived for spherical or cylindrical displacement-controlled cavity expansion in an infinite, homogeneous and isotropic continuum under an isotropic stress state in either un-drained or drained conditions [3,4]. The soil is modelled as an elasto-plastic medium controlled by the Mohr–Coulomb failure criterion or the Cam-clay failure criterion [3]. However, the behaviour of soil during compaction grouting is actually a pressure-controlled cavity expansion problem [4,23]. Moreover, these analytical methods do not consider cases of cyclic compaction grouting where more than one cycle of cavity

* Corresponding author. Tel.: +61 249215745; fax: +61 249216991.
E-mail addresses: Shanyong.Wang@newcastle.edu.au (S.Y. Wang), dave.chan@ualberta.ca (D.H. Chan), bckclam@cityu.edu.hk (K.C. Lam), skau@hkucc.hku.hk (S.K.A. AU).
[1] Tel.: +1 780 492 4725; fax: +1 780 492 0249/8198.
[2] Tel./fax: +852 27887238.
[3] Tel.:+852 28578552; fax: +852 25595337.

expansion is carried out [4]. Furthermore, the distribution of excess pore water pressure generated by compaction grouting depend on the initial stress state, boundary conditions and properties of the soil [3], which are difficult to accurately assess in closed form analytical solutions.

Numerical solutions are available for calculating soil consolidation around an expanding cavity. Jang et al. [16] used the finite element program ABAQUS to simulate a self-boring pressuremeter test including the strain holding stage. By modelling finite strain deformation in the soil and large scale sliding at the interface between the penetrometer and the soil, the cone penetration process was simulated successfully by Huang et al. [17]. Sheng et al. [18] reported the finite element analysis of pile installation using large-slip frictional contact. Kim et al. [19] used finite-element modelling and beam-column modelling of ground anchors to investigate the load transfer mechanism in ground anchors. Based on the Arbitrary Lagrangian Euler method, cone penetration in cohesive soils has been studied by Liyanapathirana [20]. However, very few numerical studies have been carried out on compaction grouting into completely decomposed granite (CDG) soils.

In this study, numerical simulations and laboratory experimental tests were carried out to provide a better understanding of the consolidation deformation and shear strength enhancement characteristics of CDG soils in Hong Kong using compaction grouting. The main advantage of small scale laboratory tests and numerical modelling is that many details of the model can be fully controlled. In addition, the soil selected for this study has been characterised with supporting laboratory data. Moreover, the boundary and loading conditions are well defined and the drainage conditions at the boundaries can be controlled. In this study, laboratory-scale "ideal compaction grouting" experiments, i.e., no occurrence of bleeding or solid penetration during the grouting process, are performed and soil behaviour during the cavity expansion is investigated. Biot consolidation processes are simulated using the finite element method. Consolidation behaviour of the soil around the expanding cavity is examined. The experimental data are compared with a numerical simulation to verify the numerical model. Factors affecting compaction efficiency are studied using the validated numerical model.

2. Laboratory tests for ideal cavity expansion test

Fig. 1 shows the schematic layout of the ideal compaction grouting (cavity expansion) experimental tests [23]. The diameter and height of the specimens are 100 mm and 200 mm, respectively. The soil was compacted in a triaxial apparatus to obtain the desired initial void ratio. Confining pressure was applied to the specimen, which was surrounded by a rubber membrane. Confining pressure and pore water pressure were measured using Transducers 1 and 2, respectively (shown in Fig. 1). Water was injected into the specimen from the bottom of the triaxial cell to achieve full saturation. The injection needle was located in the centre of the specimen. Water could enter and expand the membrane/balloon through a hole at the end of the steel injection tube. This technique of has been used by Au [4] to simulate ideal compaction grouting in the laboratory.

In addition to measuring confining pressure and pore water pressure in the soil using Transducers 1 and 2, injection pressure was measured using Transducer 3 (shown in Fig. 1). When the membrane is expanded by the injection of water, it is needed to first overcome the effect of the confining pressure applied on the soil. Further increases in pressure will cause an expansion of the membrane, which will compact and densify the surrounding soil [9,23]. Due to an increase in injection pressure, excess pore water pressure is generated which will be subsequent dissipated with time. The amount of drained water was measured using Transducer 4 (shown in Fig. 1). Transducer 4 performed two functions:
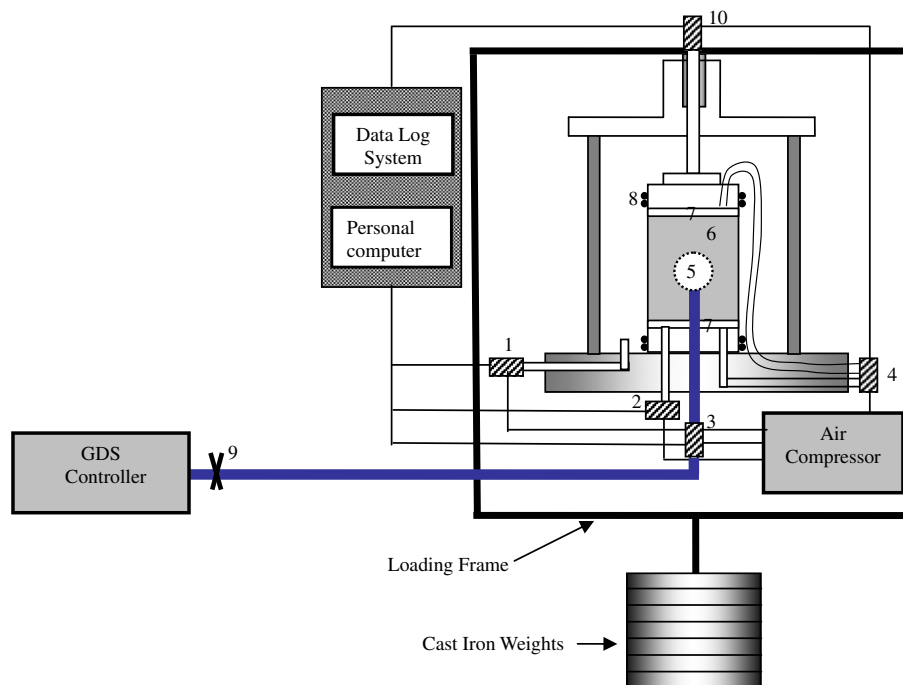
Notes:
1: Confining pressure transducer, 2: Pore water pressure transducer, 3: Injection pressure transducer, 4: Back pressure transducer, 5: Balloon, 6: Soil specimen, 7: Porous stone, 8: O ring, 9: Tap, 10: LVDT

Fig. 1. Schematic layout of static and dynamic compaction grouting experimental apparatus [23].

one to control the back pressure during the saturation process; the other function is to measure the volume change during the drained test when the back pressure transducer was turned off [23]. During the injection process, the injection pressure (p) and the injection rate (q) were also measured. Water injections were carried out using a pressure/volume controller, which controlled the injection rate and volume. Vertical displacement of the specimen was measured using a linear voltage differential transformer (LVDT). Finally, different coefficients of earth pressure (K) were created using a dead weight loading mechanism. All data collected from the transducers were automatically recorded using a data logging system [9,23].

Soil samples for the compaction grouting tests should be prepared in such a way that they are quite reproducible. The sample should achieve a predetermined dry density and should be homogeneous. More details about sample preparation can be found in [9].

The testing procedure was divided into four steps [23]. The first step was saturation of the specimen, which was necessary to provide reliable measurements of the volume change in drained or undrained tests. By flushing the sample with carbon dioxide before filling it with water the pore pressure response, parameter B, was found to be 0.98–1.00, indicating that the samples were properly saturated. The second step was the consolidation of the specimen to the desirable initial void ratio and effective confining pressure. During the second stage, water was not injected into the injection needle. During the third stage, water was injected through a hole at the end of the injection needle to expand the membrane, which caused compaction of the surrounding soils. The final step was allowing consolidation of the soil until the back pressure and pore pressure reached equilibrium ($\Delta u \approx 0$), i.e., until consolidation was completed. See [9] for more details on the experimental setup.

The soil used in this study, approximately 2 m^3, was excavated from a construction site at Beacon Hill, Kowloon Tong, Hong Kong. The natural water content of the soil was approximately 8%. The liquid and plastic limits were 36% and 25%, respectively. The optimum moisture content was 11%, which was determined using a Standard Proctor compaction test. The permeability of the soil was estimated to be 1.16×10^{-6} m/s. The maximum void ratio (e_{max}) was 1.096 and the minimum void ratio (e_{min}) was 0.493.

Table 1 summarises the physical properties of the extracted CDG soil [22,23].

3. Finite element simulations of ideal compaction grouting tests

The commercial finite-element code ABAQUS/Standard was used to perform the numerical simulations of the ideal compaction grouting (cavity expansion) tests [21]. An isotropic elasto-plastic model using the Mohr–Coulomb failure criterion with a non-associated flow rule was adopted. The model was expressed in terms of stress invariants in ABAQUS [21]. In this model, the Young's modulus, Poisson's ratio, cohesion, friction angle and dilation angle must be provided by the user. Void ratio can be related to volumetric strain [21]. The properties for CDG soil in Hong Kong used in the finite element models are summarised in Table 2.

The analysis of the ideal compaction grouting was treated as a two-dimensional axisymmetric problem. Eight-node axisymmetric pore pressure elements with reduced integration (ABAQUS element type CAX8RP) were used in this analysis. The finite element discretisation consisted of 932 elements. The mesh was graded in the radial direction; it was finer near the injection cavity where the pressure gradient was expected to be the highest. Variations of void, permeability, stresses, strains and excess pore pressures were monitored at six selected points, as illustrated in Fig. 2. Expansion of the latex membrane provided an internal pressure around the injection cavity. A uniform pressure boundary was applied in the finite element model. In addition, the vertical right boundary and the top boundary were subjected to stress control

Table 1
Basic physical properties of Hong Kong CDG for the physical model [22,23].

Properties	Value
Natural water content	8%
Gravel	30%
Sand	64%
Fine particles (0.075 mm)	6%
D_{10}	0.18 mm
D_{30}	0.7 mm
D_{60}	1.8 mm
Coefficient of uniformity (D_{60}/D_{10})	10
Liquid limit	36%
Plastic limit	25%
Plasticity index	11%
e_{max}	1.096
e_{min}	0.493
Optimum moisture content	11%
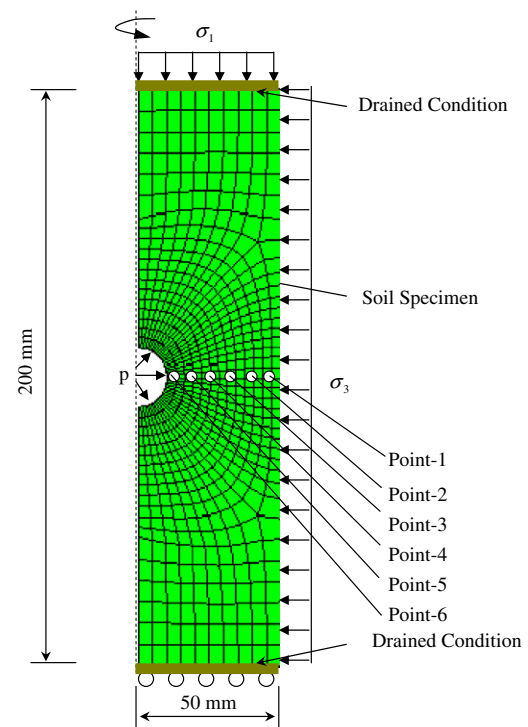
Fig. 2. Finite element axial-symmetric mesh and boundary conditions for R50 compact injection tests using ABAQUS 6.3.

Table 2
Soil properties of Hong Kong CDG for the numerical model.

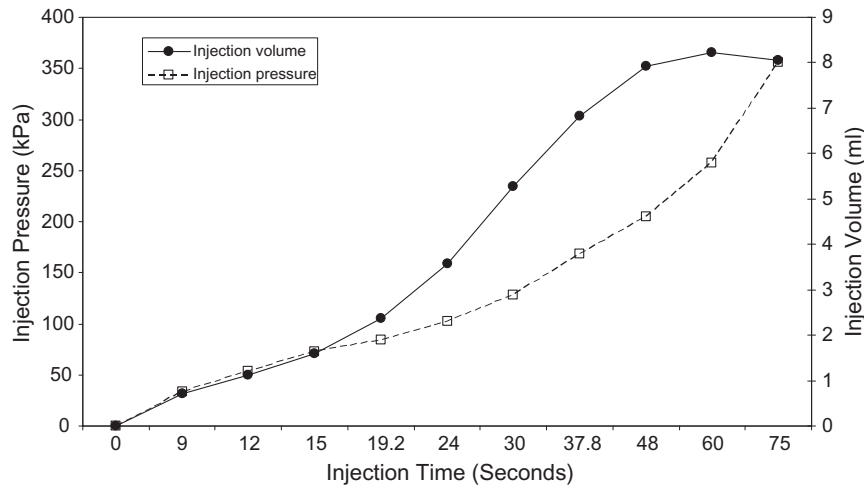|	Density	Permeability	Young's modulus	Poisson's ratio	Friction angle	Dilation angle	Cohesion
Soil	1.65 Mg/m^3	1.16E−6 m/s	14 MPa	0.34	34°	11°	26 kPa

Fig. 3. Pressure–volume responses versus time during cavity expansion.

conditions and only the bottom boundary was fixed because lateral and vertical deformations were allowed. The top and bottom boundaries were considered to be fully drained.

An initial cavity radius of 8.5 mm was used in the simulation. The nodal reaction forces around the cavity at equilibrium under the confining pressure were calculated first. The same forces were then applied at the nodes to maintain the initial spherical shape of the cavity, which simulated the stresses applied on the injection needle due to the confining pressure. The area inside the boundary around the cavity was allowed to deform before the application of the injection pressure [3,4]. After the application of the confining pressure, injection was modelled by applying injection pressure around the spherical cavity to create a cavity expansion. Injection pressure and injection volume versus time, measured from the experimental test, are shown in Fig. 3. Due to the use of Biot's theory of consolidation in ABAQUS, a realistic estimation of time dependent behaviour can be obtained from the numerical simulations.

4. Comparison of experimental results with numerically simulated results

In order to compare the experimental and numerical simulation results, it is necessary to define a criterion for evaluating the degree of compaction. Hence, assuming that the sandy soil is totally saturated, the effect can be expressed by the change in mean void ratio of the soil ($\Delta \bar{e}$). Because the maximum void ratio (e_{max}) and the minimum void ratio (e_{min}) can be measured beforehand [22,23], the compaction grouting efficiency η^*, is defined as follows:

$$\eta^* = \frac{\Delta \bar{e}}{e_{max} - e_{min}} \tag{1}$$

where $\bar{e}$ is the average void ratio, and it is calculated from $\bar{e} = e_0 - \Delta \bar{e}$. e_0 is the initial void ratio, which can be controlled in the test and $\Delta \bar{e}$ is measured from the volume of drained water in the test. In addition, based on the definition of compaction grouting efficiency, the average un-drained strength enhancement ratio $\bar{\alpha}$ can be derived as follows [9,23]:

$$\bar{\alpha} = \exp\left(\frac{(e_{max} - e_{min}) \cdot \eta^*}{\lambda}\right) \tag{2}$$

where λ is the gradient of the normal consolidation line in e–ln p' space [24], which can be measured from the triaxial test. Since the geotechnical engineer is often more concerned about the overall performance of the soil in a site, in the current study, the average un-drained shear strength enhancement ratio of a soil specimen, as defined in [3], was used. A greater change (reduction) in void ratio results in a greater increase in un-drained shear strength of the soil.

To minimise variability in the experimental results, three pressure-controlled compaction grouting laboratory tests were conducted to evaluate the validity of the numerical model. The experimental results presented here are an average of the three tests. The consolidation process was finished within 30 min [9]. Simulated consolidation calculations were stopped after 30 min, which was the duration observed in the laboratory experimental tests. It is difficult to monitor void ratio change and pore water pressure distribution at every point in the soil due to cavity expansion in experimental tests. As such, the experimental result presented here is the average change of void ratio of the sample. However, numerical modelling has the advantage of providing information about every point.

Both the numerical and experimental results on void ratio changes with time are shown in Fig. 4. The calculated void ratio at points oriented radially from the injection cavity decreases gradually and the total void ratio change also decreases for each cycle. These findings were also observed in the experiment. At locations close to the injection cavity, void ratio changes were larger. For example the total normalised void ratio change, e/e_0, for Point 6 (close to the injection cavity, Fig. 2) is about 0.17. In comparison, the void ratio change for Point 1 (farthest from the injection cavity, Fig. 2) is nearly zero, which indicates that the influence of radius due to cavity expansion does not exceed the radius of the sample. In addition, the average void ratio change of all six points for the corresponding experiment was about 0.07. This is similar to the experimental result which had a mean void ratio change of 0.069. This similarity suggests that the numerical model effectively to simulate the experimental tests.

Based on Eq. (1), Fig. 5 illustrates the calculated compaction efficiency for the normalised radial distance, which is defined as the ratio of the distance from the injection cavity to the initial radius of the injection cavity. From Fig. 5, the compaction efficiency is the highest near the injection cavity and decreases gradually from 0.237 to 0.007 as you move away from injection cavity. Similarly, from Eq. (2), the mean shear strength enhancement ratio in Fig. 6 represents the same trend as the compaction efficiency shown in Fig. 5. The mean shear strength enhancement ratio also decreases radially from the injection cavity. The highest mean shear strength enhancement ratio is 4.5, and the lowest mean shear strength enhancement ratio is 1.0. In addition, both the compaction efficiency and the shear strength increase more promi-
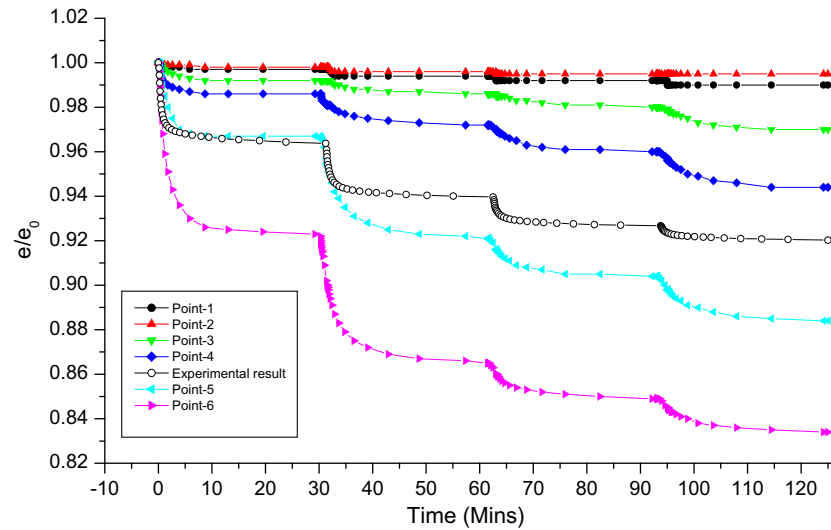
Fig. 4. Numerical and experimental results of e/e_0 versus time for the radial distance from the injection cavity (time is continuous from the first injection to the end of the fourth consolidation).
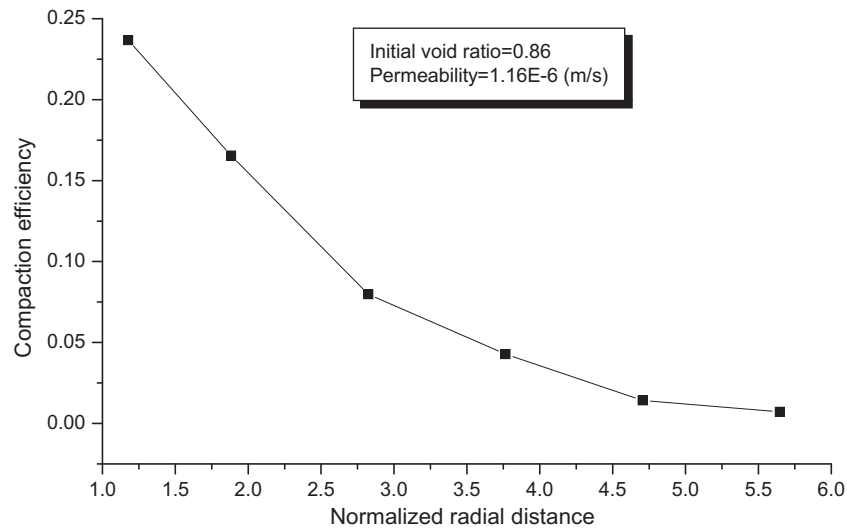
Fig. 5. Numerically simulated results of compaction efficiency for normalised radial distances from the injection cavity.
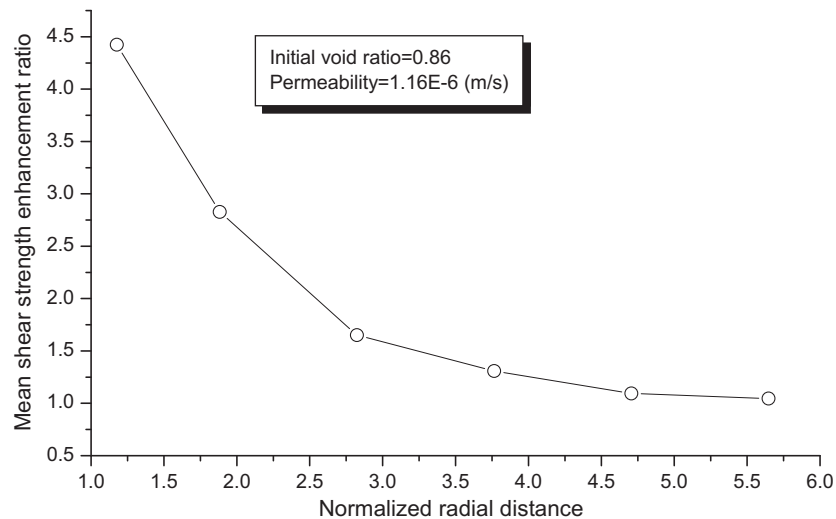
Fig. 6. Numerically simulated results of mean shear strength enhancement ratios for normalised radial distances from injection cavity.

nently close to the injection cavity, which can be seen from the gradient of their trends being higher at the cavity and then becoming steady as shown in Figs. 5 and 6.

Fig. 7 shows the pore water pressure versus time for different radial distances. During the process of cavity expansion and subsequent consolidation of the soil, the pore pressure usually increases suddenly and then drops rapidly until it levels off to a steady value, which indicates that consolidation is finished. Furthermore, the closer the distance to the injection cavity the higher the peak pore water pressure at a given point.

5. Numerical results and discussions

5.1. Effect of the coefficient of earth pressure (K) on compaction efficiency

In this section, the effect of the coefficient of earth pressure (K) on compaction grouting efficiency is studied, based on the material

parameters calibrated using the experimental data discussed above. K ranges from 0.6 to 1.4. K is changed by keeping the vertical stress constant and changing the confining pressure. The initial void ratio is 0.86. It is difficult for laboratory tests to control the boundary condition for a specimen when $K > 1$. However, numerical simulations do not have such limitations. All plots shown in this section are taken from Point 4, which is located in the middle of the monitoring points. Point 4 was selected because it represents the mean response of the soil.

Fig. 8 shows the numerical results of e/e_0 versus time for different values of K. The normalised void ratio change is highly affected by K; the higher the value of K, the smaller the normalised void ratio change. Based on Eq. (1), the compaction efficiency decreased from 0.233 to 0.078 when K increased from 0.6 to 1.4 (Fig. 9). Similarly, based on Eq. (2), the mean shear strength enhancement ratio decreased from 4.325 to 1.629 when K increased from 0.6 to 1.4 (Fig. 10). Fig. 11 shows simulated pore water pressure versus time for three selected values of K (0.6, 1.0 and 1.4). From Fig. 11, it is
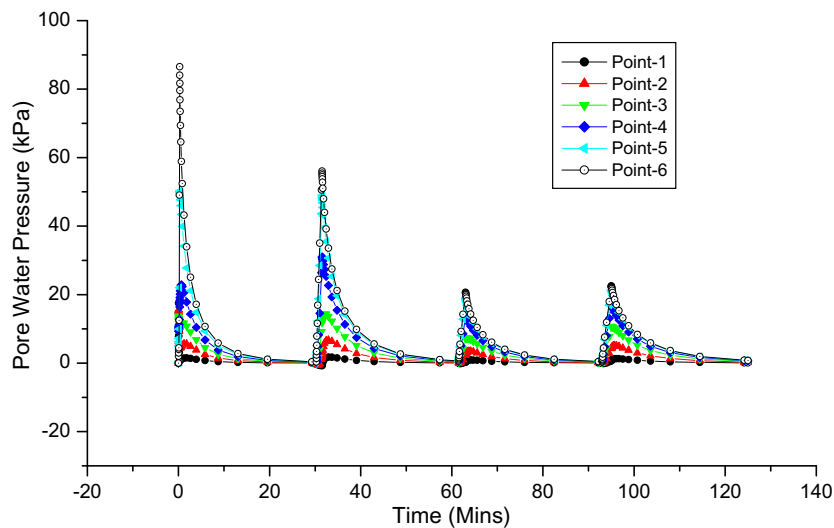

Fig. 7. Numerical simulated results of pore water pressure versus time for six selected points.
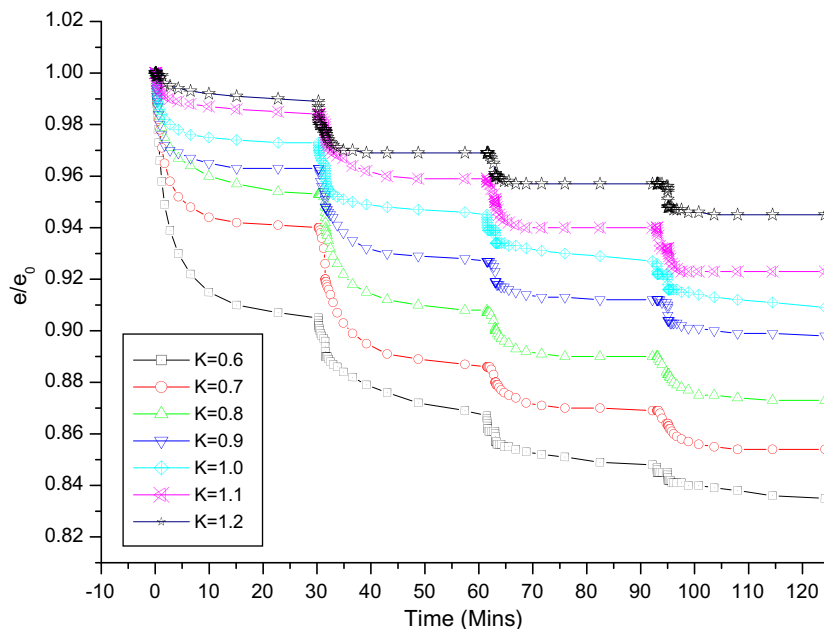

Fig. 8. Numerically simulated results of e/e_0 versus time for different coefficients of earth pressure (K).
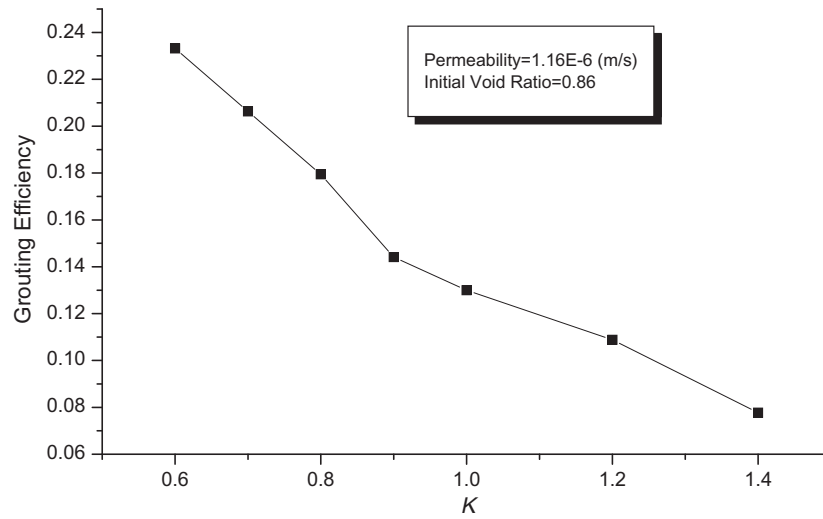
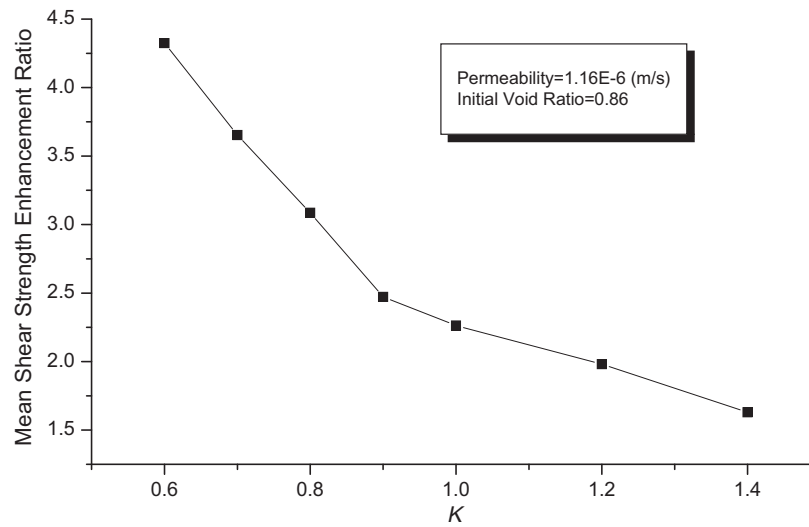**Fig. 9.** Numerically simulated results of compaction efficiency versus the coefficient of earth pressure (*K*).

Fig. 10. Numerically simulated results of mean shear strength enhancement ratio versus the coefficient of earth pressure (*K*).
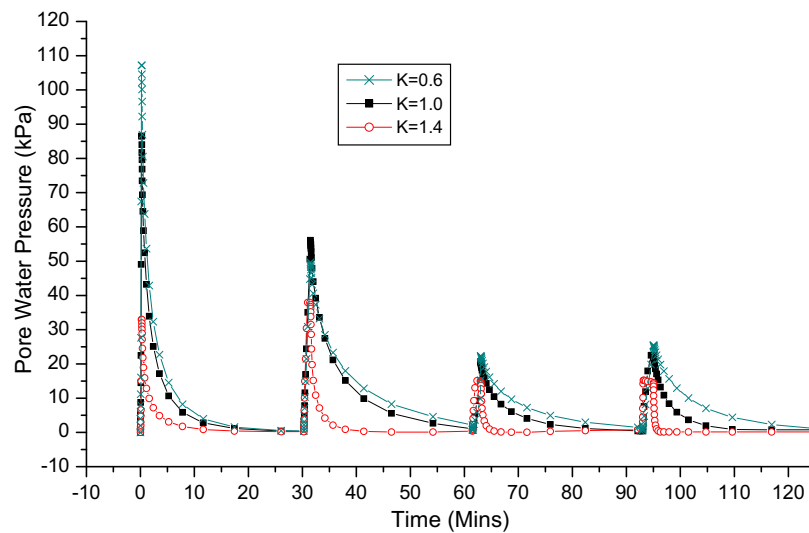

Fig. 11. Numerically simulated results of pore water pressure versus time for different coefficients of earth pressure (*K* = 0.6, 1.0 and 1.4).

apparent that pore water pressure decreases with increasing K. This is due to the confining pressure decreasing gradually with increasing K, although the input injection pressure is kept the same for all K. The trend of the peak pore water pressure for each monitored point is the same as shown in Fig. 7.

Figs. 12 and 13 show the lateral and vertical deformation of Point 6, respectively. For Point 6, the closest selected point to the injection cavity, both the vertical and horizontal deformation increase rapidly during the initial injection period and then become steady after consolidation of the soil. The final vertical deformation for four cycles of loading is about 6–7 times the lateral deformation, for K = 1.4 ($\sigma_h' = 1.4\sigma_v'$, $\sigma_h' = 100$ kPa), which indicates that vertical deformation is larger than lateral deformation. This also indicates that the deformation of the injection cavity is not circular for this case. This phenomenon was verified by the experimental tests that showed the injection balloon was not circular when K was not equal to 1 [4,9].

5.2. Effect of initial void ratio on compaction efficiency

In order to evaluate the effects of different void ratios on compaction efficiency, a series of numerical simulations were carried out. For these simulations K was equal to one. The initial void ratios were 0.55, 0.6, 0.7, 0.8, 0.9, and 0.95. Fig. 14 shows the void ratio change versus time for different initial void ratios. For the cases with initial void ratios of 0.95, 0.9 and 0.8, the void ratio changes were much higher than for the cases with initial void ratios of 0.7, 0.6 and 0.55. It seems that the smaller the initial void ratio, the smaller the void ratio changes. This phenomenon can be seen more clearly in Fig. 15, which shows the relationship between relative density and initial void ratio. Relative density is commonly used to indicate the density of granular soil. For initial void ratios of 0.95, 0.9, 0.85 and 0.8, the corresponding initial relative densities were 0.24, 0.32, 0.40 and 0.49, respectively, and the final relative densities were 0.48, 0.57, 0.64 and 0.72, respectively.
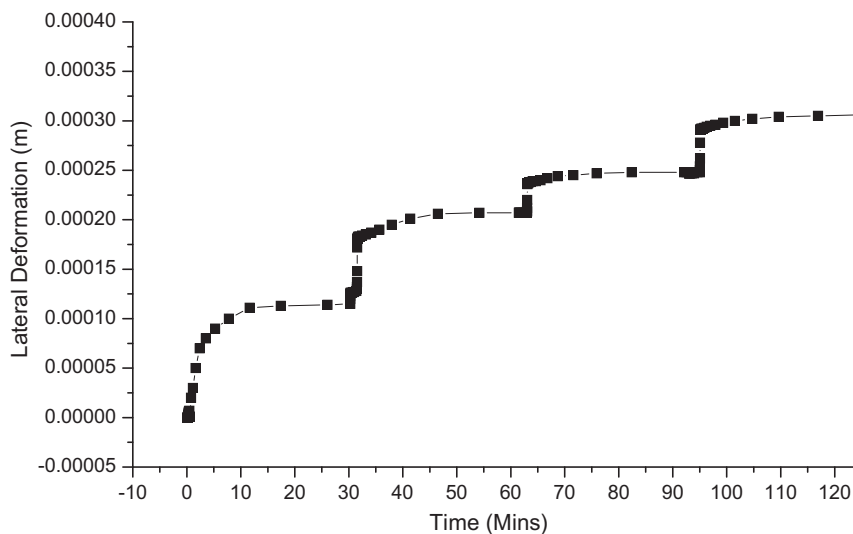

Fig. 12. Numerically simulated results of lateral deformation versus time for coefficient of earth pressure K = 1.4.
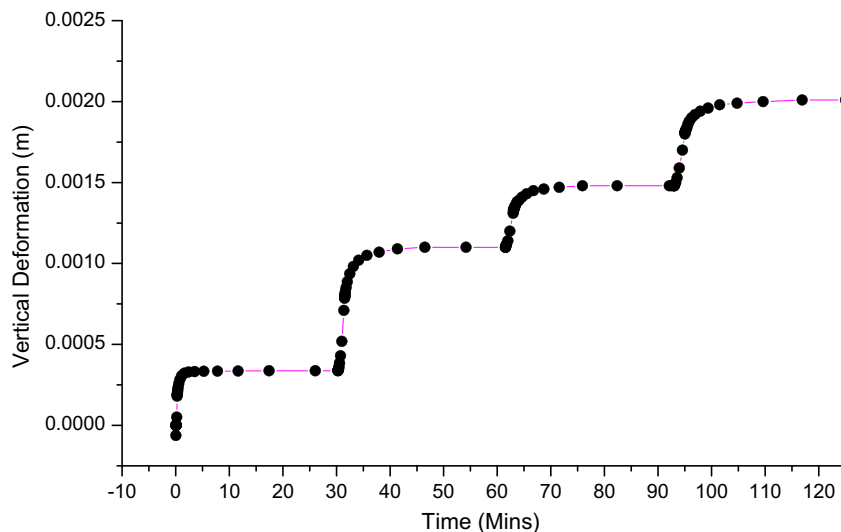

Fig. 13. Numerically simulated results of vertical deformation versus time for coefficient of earth pressure K = 1.4.
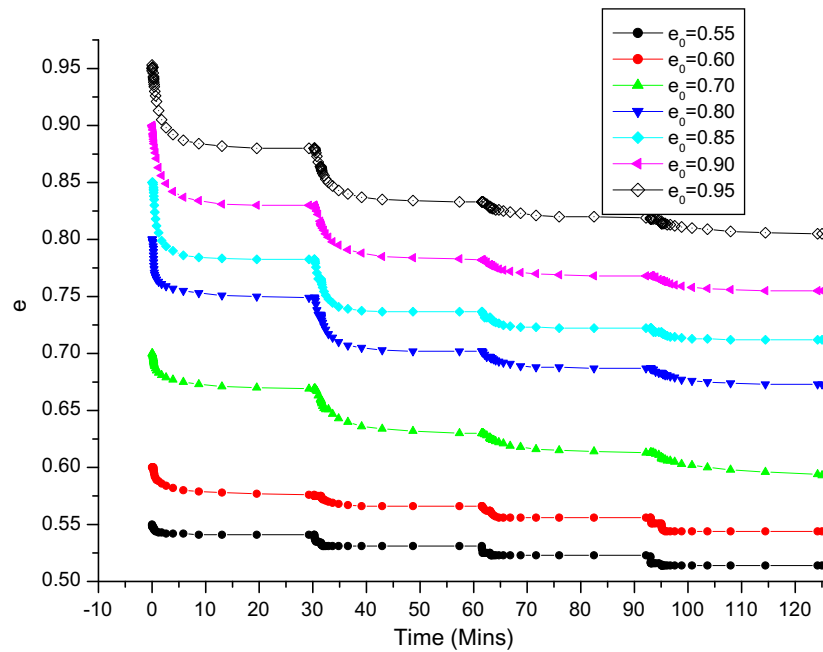
Fig. 14. Void ratio changes versus time for the different initial soil void ratios.
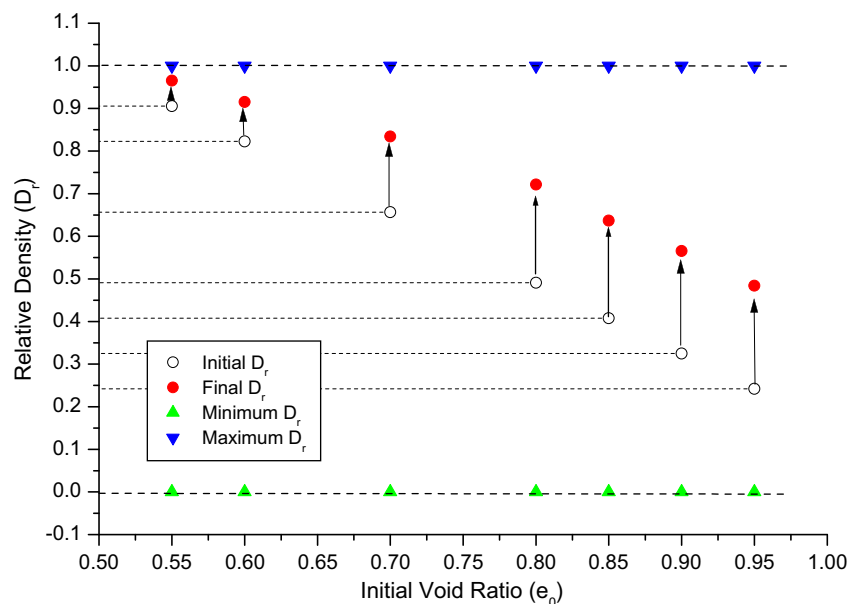

Fig. 15. Numerically simulated results of relative density versus initial void ratio of soils.

Generally, soils with these initial void ratios are loosened and it is easier for such soils to be further densified. As shown in Fig. 15, changes in relative density are higher (indicated by longer arrows in the figure) for cases with initial void ratios of 0.95, 0.9, 0.85 and 0.8 than the other three cases with initial void ratios of 0.7, 0.6 and 0.55. This is due to the fact that soils with initial void ratios of 0.7, 0.6 and 0.55 are denser than those with initial void ratios of 0.9, 0.82 and 0.66. It is relatively more difficult for these soils to be further densified.

Figs. 16 and 17 show the compaction efficiencies and mean shear strength enhancement ratios versus initial void ratios of soils, respectively. The compaction efficiencies and mean shear strength enhancement ratios increase prominently when the initial void ratios increases from 0.55 to 0.7, and then becomes steady from 0.8 to 0.95. This indicates that for looser soil, the initial void ratio does not significantly affect the compaction efficiency and the mean shear strength enhancement. For denser soils, the initial void ratios have a stronger influence on the compaction efficiency and mean shear strength enhancement ratio.

5.3. Effect of loading cycles on the compaction efficiency

In this section, a series of numerical simulations were carried out to evaluate the effect of different loading cycles on compaction efficiency. The number of cavity expansion cycles ranged from 1 to 8. For each cycle of loading, the injection pressure was kept the
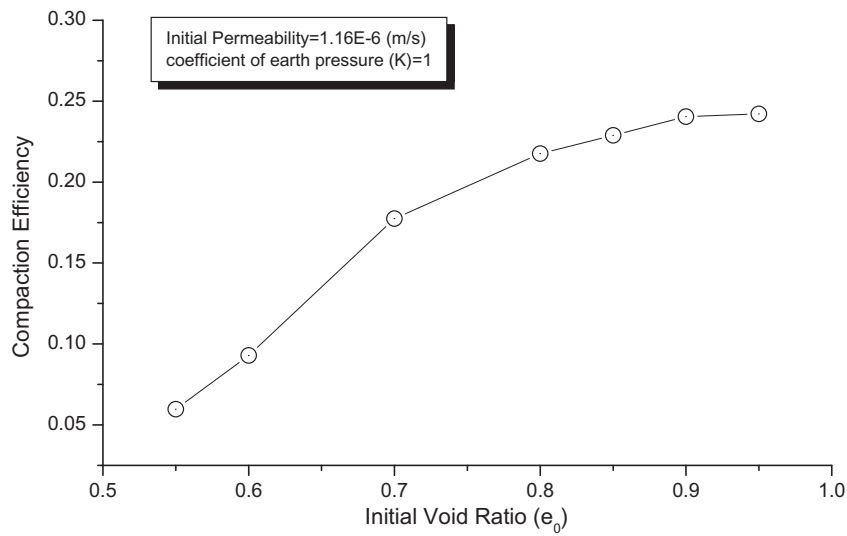
Fig. 16. Numerically simulated results of compaction efficiency versus initial void ratio of soils.
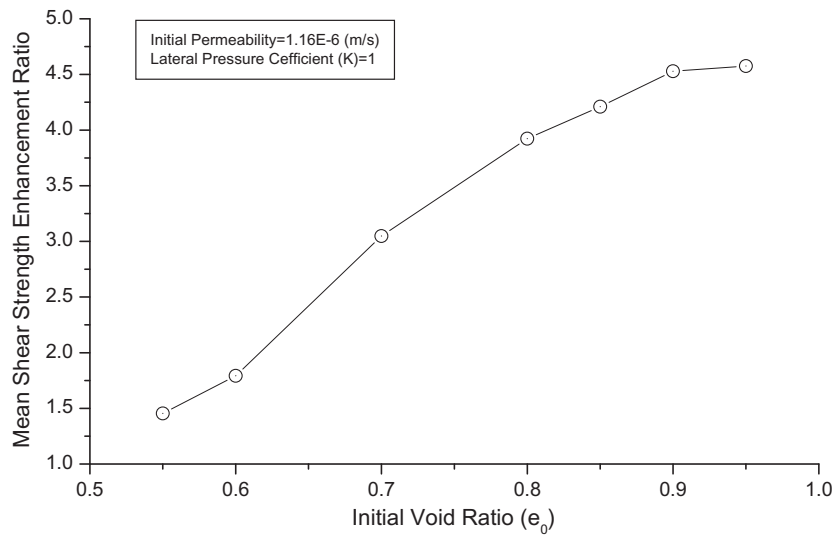

Fig. 17. Numerically simulated results of mean shear strength enhancement ratio versus initial void ratio of soils.
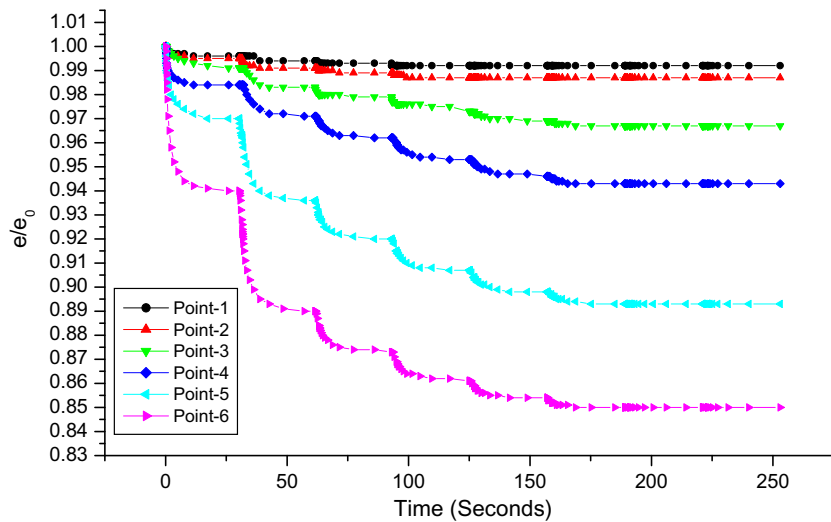

Fig. 18. Numerically simulated results of normalised e/e_0 versus time for the six monitored points due to eight cycles of cavity expansions.

same (Fig. 3). For this analysis, *K* was equal to one and the initial void ratio was 0.86. Fig. 18 shows the numerical results of e/e_0 versus time for all six points for eight cycles of loading. The normalised void ratio changes decrease gradually with each cycle of loading until there is almost no change in the eighth cycle of loading. Fig. 19 shows the numerical results of pore water pressure versus time for Points 4, 5 and 6. Peak pore water pressure decreases with each cycle of loading.

Figs. 20 and 21 show the numerically simulated compaction efficiencies and mean shear strength enhancement ratios of Points, 4, 5 and 6 versus the cycles of loading. Compaction efficiency and mean shear strength enhancement increase gradually with

increasing cycles of loading, until they reach an upper limit. The above analysis indicates that more cycles do not result in better compaction efficiency. This knowledge can be used to determine the optimum cycle of loading for maximum compaction efficiency with minimum effort. In the present case, the optimum number of cycles is 5.

5.4. Effect of effective confining pressure on compaction efficiency

A series of numerical simulations were carried out to evaluate the effect of confining pressure on compaction efficiency. Four cycle of loading was used and the initial void ratio was 0.86. The
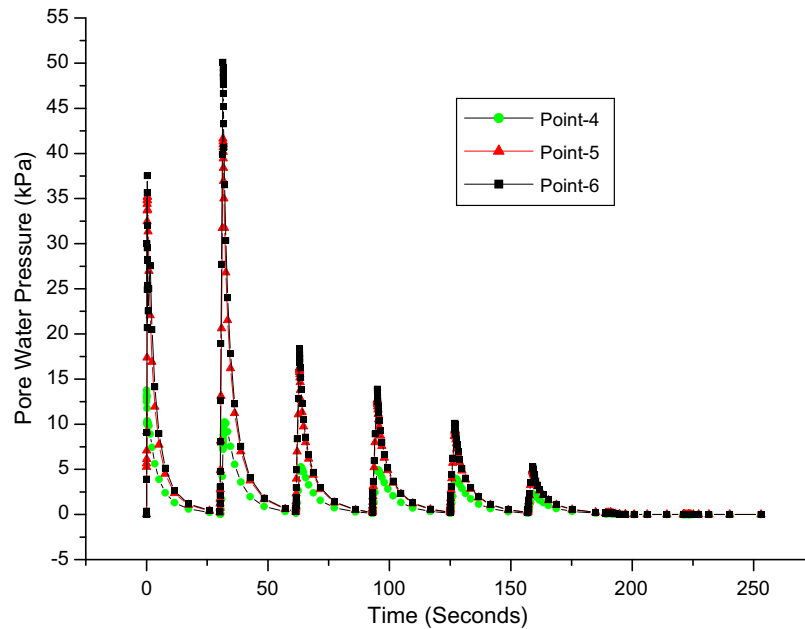

Fig. 19. Numerically simulated results of pore water pressure versus time for Points 4, 5 and 6 (Fig. 2) due to eight cycles of cavity expansion.
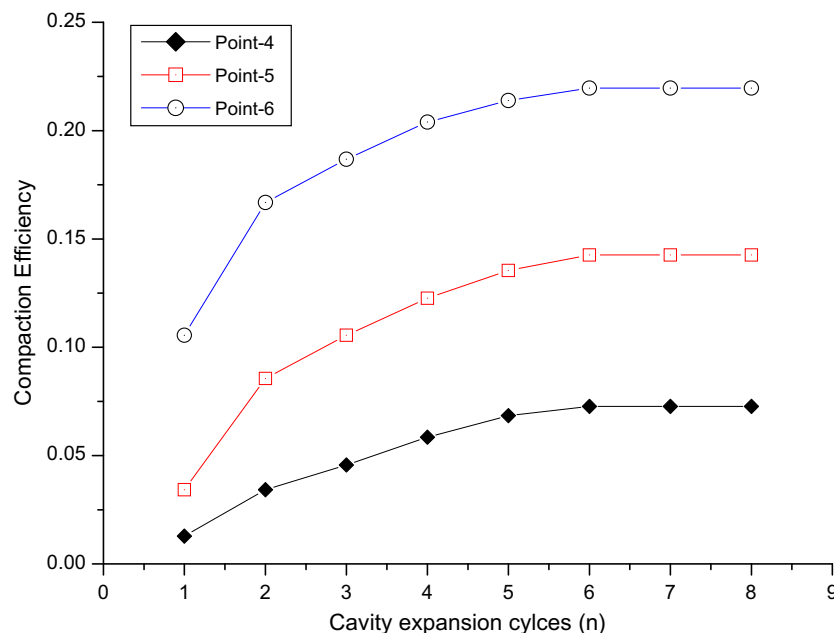

Fig. 20. Numerically simulated results of compaction efficiency versus cavity expansion cycle for Points 4, 5 and 6 (Fig. 2).
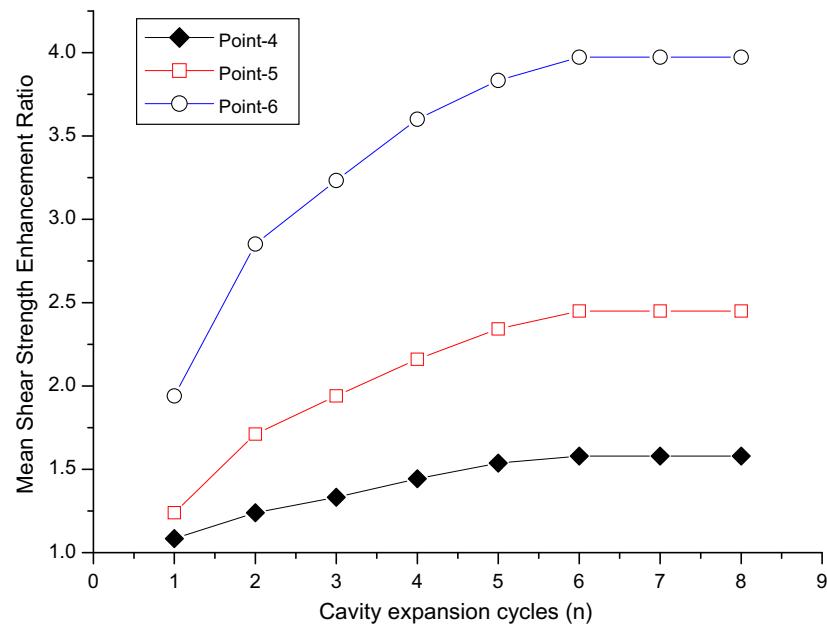
Fig. 21. Numerically simulated results of mean shear strength enhancement ratio versus cavity expansion cycles for Points 4, 5 and 6 (Fig. 2).
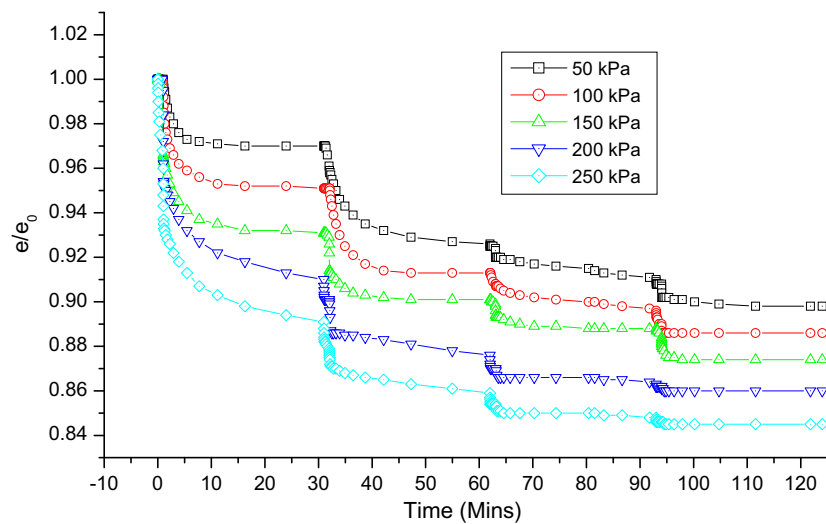

Fig. 22. Numerically simulated results of e/e_0 versus time for different effective confining pressures at Point 4 (Fig. 2).
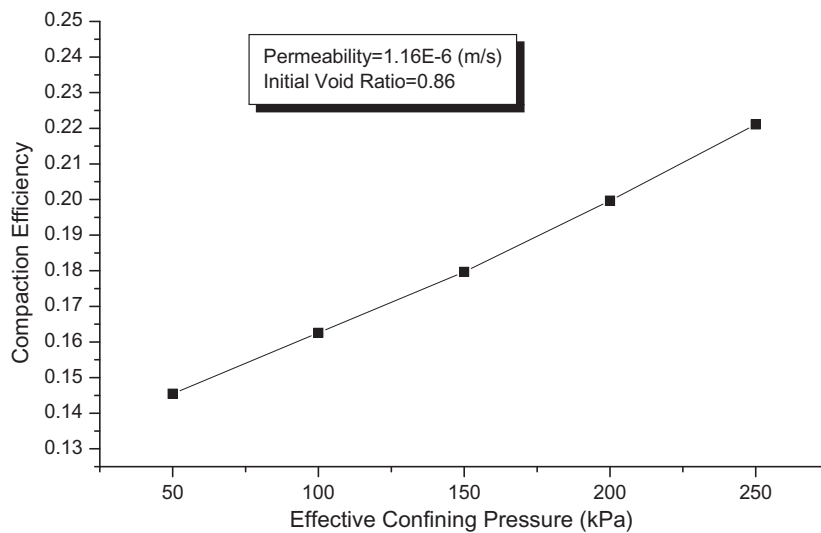

Fig. 23. Numerically simulated results of compaction efficiency versus effective confining pressure at Point 4 (Fig. 2).
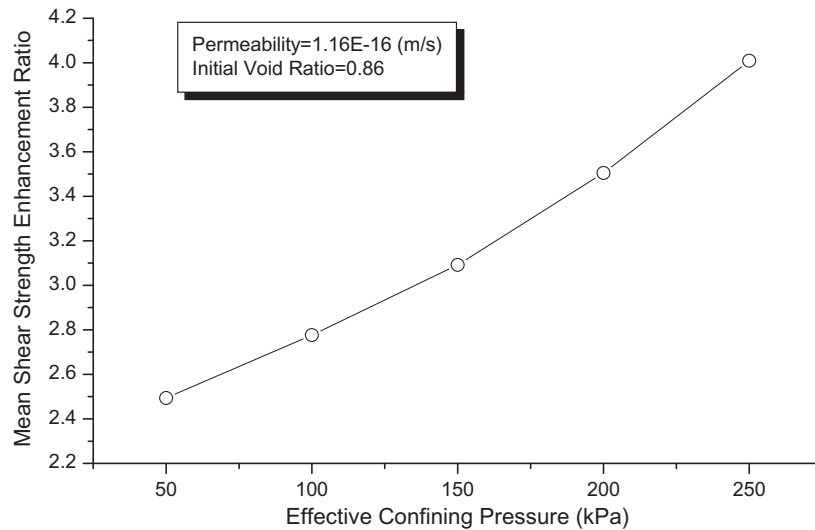
Fig. 24. Numerically simulated results of mean shear strength enhancement ratio versus effective confining pressure at Point 4 (Fig. 2).

effective confining pressure ranged from 50 to 250 kPa. Fig. 22 shows the normalised void ratio e/e_0 versus time for different confining pressures. Usually, the effective confining pressure reflects the injection depth [9]. The higher the effective confining pressure the deeper the injection depth. Therefore, void ratio changes in Fig. 22 reflect the effect of the injection depth on the compaction efficiency. Fig. 22 shows the normalised void ratio change decreases with increasing effective confining pressure, which indicates that the soil can be densified more effectively with an increase in injection depth. Fig. 23 shows the relationship between compaction efficiency and effective confining pressure. The compaction efficiency increases almost linearly with increase in confining pressure. Moreover, the mean shear strength enhancement ratio, shown in Fig. 24, reflects the trend shown in Fig. 23.

6. Conclusions

To study the ideal compaction grouting (cavity expansion) in CDGs of Hong Kong, a triaxial apparatus was introduced. Using this apparatus, laboratory scaled pressure-controlled cavity expansion tests were carried out. In addition, compaction efficiency was defined as a measure of the effectiveness of soil compaction. The results from the experimental tests were compared with a finite element simulation and were used to validate the finite element solutions.

Numerical simulations of soil behaviour during cavity expansion and Biot consolidation processes were conducted using finite element analyses. Experimental and numerical results showed that the compaction efficiency decreases when the coefficient of earth pressure (K) increases from 0.6 to 1.4. Numerical results show that the compaction efficiency decreases as the initial void ratio increases from 0.55 to 0.95. The initial void ratios influence the compaction efficiency for denser soils more than looser soils. Moreover, compaction efficiency increases gradually with an increase of the number of cycles of cavity expansions, until it reaches an upper limit. Thus, an optimum number of loading cycles can be determined for maximum compaction efficiency with minimum effort. Finally, the compaction efficiency increases almost linearly with increases in confining pressure.

References

[1] Graf ED. Compaction grouting technique. J Soil Mech and Found Div, ASCE 1969;95(5):1151–8.
[2] Warner J, Brown DR. Planning and Performing Compaction Grouting. J Soil Mech Found Div, ASCE 1974;100:653–66. GT6, Proc. Paper 10606.
[3] Au SKA, Yeung AT, Soga K, Cheng YM. Effects of subsurface cavity expansion in clays. Geotechnique 2007;57(10):821–30.
[4] Au SKA. Fundamental study of compensation grouting. PhD dissertation, Department of Engineering, University of Cambridge, Cambridge, England; 2001.
[5] Au SKA, Soga K, Jafari MR, Bolton MD, Komya K. Factors affecting long-term efficiency of compensation grouting in clay. J Geotech Geoenviron Eng, ASCE 2003;129(3):354–62.
[6] Soga K, Au SKA, Jafari MR, Bolton MD. Laboratory investigation of multiple grout injections into clay. Geotechnique 2004;54(2):81–90.
[7] Carter JP, Randolph MF, Wroth CP. Stress and pore pressure changes in clay during and after the expansion of a cylindrical cavity. Int J Numer Anal Methods Geomech 1979;3:305–22.
[8] Collins IF, Pender MJ, Wang Y. Cavity expansion in sands under drained loading conditions. Int J Numer Anal Methods Geomech 1992;16:3–23.
[9] Wang SY. Fundamental study of static and dynamic compaction grouting in complete decomposed granite, PhD dissertation, City University of Hong Kong, PR China; 2006.
[10] Carter JP, Booker JR, Yeung SK. Cavity expansion in cohesive-frictional soils. Geotechnique 1986;36:349–58.
[11] Collins IF, Stimpson JR. Similarity solutions for drained and undrained cavity expansions in soils. Geotechnique 1994;44:21–34.
[12] Yu HS, Houlsby GT. A large strain analytical solution for cavity contraction in dilatant soils. Int J Numer Anal Mech Geomech 1995;19(7):793–811.
[13] Cao LF, Teh CI, Chang MF. Undrained cavity expansion in modified Cam clay. Geotechnique 2001;51:323–34.
[14] Osinov VA, Cudmani R. Theoretical investigation of the cavity expansion problem based on a hypoplasticity model. Int J Numer Anal Methods Geomech 2001;25:473–95.
[15] Russell AR, Khalili N. Drained cavity expansion in sands exhibiting particle crushing. Int J Numer Anal Methods Geomech 2002;26:323–40.
[16] Jang IS, Chung CK, Kim MM, Cho SM. Numerical assessment on the consolidation characteristics of clays from strain holding, self-boring pressure pressuremeter test. Comput Geotech 2003;30:121–40.
[17] Huang W, Sheng D, Sloan SW, Yu HS. Finite element analysis of cone penetration in cohesionless soil. Comput Geotech 2004;31:517–28.

[18] Sheng DC, Eigenbrod KD, Wriggers P. Finite element analysis of pile installation using large-slip frictional contact. Comput Geotech 2005;32:17–26.

[19] Kim NK, Park JS, Kim SK. Numerical simulation of ground anchors. Comput Geotech 2007;34:498–507.

[20] Liyanapathirana DS. Arbitrary Lagrangian Eulerian based finite element analysis of cone penetration in soft clay. Comput Geotech 2009;36:851–60.

[21] Hibbitt, Karlsson, Sorensen, Inc., ABAQUS theory manual, Version 6.3; 2003.

[22] Wang SY, Chan D, Lam KC. Experimental study of the effect of fines content on dynamic compaction grouting in completely decomposed granite of Hong Kong. Constr Build Mater 2009;23(3):1249–64.

[23] Wang SY, Chan DH, Lam KC, Au SKA. Effect of lateral earth pressure coefficient on pressure controlled compaction grouting in triaxial condition. Soils Found 2010;50(3):441–5.

[24] Wood DM. Soil behaviour and critical state soil mechanics. Cambridge: Cambridge University Press; 1991.